Journal of Colloid and Interface Science 566 (2020) 120–134

Contents lists available at ScienceDirect

Journal of Colloid and Interface Science

journal homepage: www.elsevier.com/locate/jcis

Controllable fabrication of biodegradable Janus and multi-layered particles with hierarchically porous structure

Agni Kumar Biswal, Sampa Saha *

Department of Materials Science and Engineering, Indian Institute of Technology, Delhi 110016, India

GRAPHICAL ABSTRACT

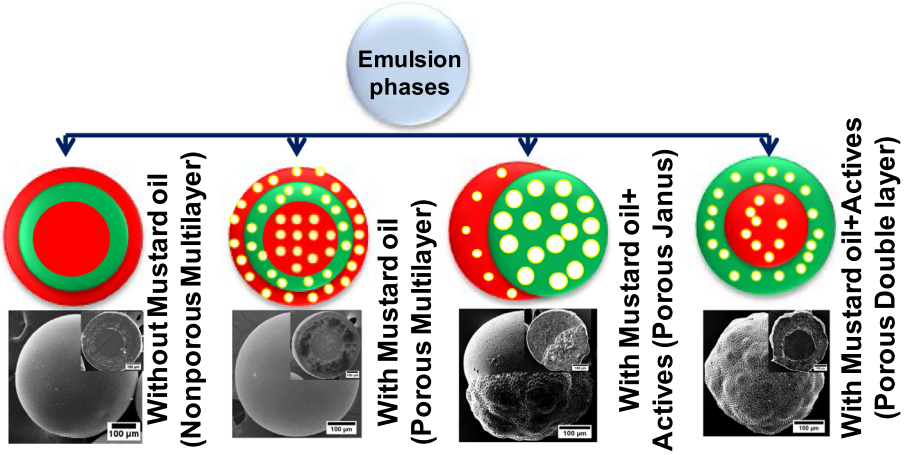

ARTICLE INFO

Article history:
Received 29 October 2019
Revised 15 January 2020
Accepted 19 January 2020
Available online 21 January 2020

Keywords:
Emulsion
Polymeric Janus microparticles
Porosity
Controlled release
Antibacterial and Antioxidant

ABSTRACT

We introduce a facile strategy to synthesize both Janus and multi-layered microparticles with hierarchically porous structure by adopting a simple oil-in-water emulsion technique. Incorporation of a minute quantity of non volatile poor solvent such as mustard oil into the emulsion comprising of biodegradable polymers such as Poly(lactic-*co*-glycolic acid)(PLGA) and Poly(L-lactic acid)(PLLA), led to a precisely controlled phase separation. This resulted in the formation of Janus or multi-layered particles with hierarchically porous structure depending on the amount of mustard oil and viscosity/crystallinity of the polymers employed. No additional toxic porogen needs to be added to induce the porosity. The mechanism of formation of various architectures was explored with the supportive evidences primarily from in situ optical microscopy along with interfacial tension measurements. Moreover, we also show the potential application of these unique particles in delivering multiple actives by encapsulating and releasing the dual actives (antibacterial and antioxidant) in controlled fashion for prolonged period of time (60 days). The release profiles of the dual actives were found to be influenced by the porosity as well as architecture of the particles.

© 2020 Elsevier Inc. All rights reserved.

* Corresponding author.
E-mail address: ssaha@polymers.iitd.ac.in (S. Saha).

https://doi.org/10.1016/j.jcis.2020.01.071
0021-9797/© 2020 Elsevier Inc. All rights reserved.

1. Introduction

Microparticles with controllable architecture have drawn immense attention due to their various functionalities and ability to release actives in targeted/triggered and/or programmed fashion [1–7]. Recently, among the emerging particles with various shape/size/phase/functionality, multi-layered particles and anisotropic particles have been exploited significantly because of their unique shape and fascinating properties [8–13]. Multi-layered polymeric particles consist of concentric layers of different polymers which are immiscible to each other above the cloud point [8]. The layers present in the particles provide distinctly different release profiles of the actives encapsulated in each layer. Moreover, actives can be well protected by the shell, thus minimizing the initial burst release of the active. However, anisotropic Janus particles possess two well-defined polymeric phases that co-exist in side-by-side fashion displaying a unique asymmetry within a single particle and hence offers directional functionality that is unachievable from symmetric particles [1,2,14–16]. Several fabrication methods developed so far to synthesize Janus particles include electro hydrodynamic co-jetting technique [17], microfluidics in combination with lithographic techniques [18,19], Pickering emulsions [20], seeded polymerization, particle replication in low surface energy templates [21], selective cross linking of polybutadiene segments in terpolymers [22], lithographic patterning of microspheres [23], electrochemical [24] and photochemical [25] reduction, templating of porous membranes [26,27] and nanotubes [28], surfactant aided growth [29], graft polymerization [30–32] and processes based on controlled surface nucleation [33]. However, the most sought after processes to synthesize multilayered particles are emulsion solvent evaporation method [34], layer by layer assembly [35], emulsion polymerization [36], coaxial electro spinning [37] etc. Though numerous advanced strategies exist to prepare Janus and multi-layered particles separately with partial overlap, studies related to simultaneous fabrication of multilayered and Janus particles by using similar strategy are scarce due to the difficulty in manipulating experimental parameters to achieve both. In this context, a report published by Li et al. worth a mention. They have fabricated PLGA/Polycaprolactone (PCL) Janus as well as core-shell particles using oil/water emulsion produced in microfluidic device [38]. By switching the dispersed phase (organic solvents) in the emulsion such as dimethyl carbonate and dichloromethane, both kinds of particles were successfully synthesized. The particles were devoid of significant surface porosity which is an important parameter to control the release of actives owing to its high surface area [39]. It is still a big challenge to devise a single strategy to make microparticles with hierarchical surface porosity along with controlled architectures such as either Janus or multilayered simply by tweaking experimental parameters. To the best of our knowledge, no such strategy is developed and reported so far. Recently, Peng *et al.* have demonstrated the fabrication of Janus particles with hierarchical porosity by seeded polymerization which requires multiple steps and stringent conditions as well [40]. In this submission, we describe a facile strategy to synthesize both multi-layered and Janus particles with hierarchical porosity by manipulating the interfacial tension and viscosity of polymers employed in simple oil-in-water (O/W) emulsion. The key criteria to prepare Janus and multi-layered particles would be to induce precisely controlled phase separation between two immiscible components via dewetting and wetting respectively in a simple O/W emulsion [41,42]. In this work, the requirement has been accomplished by adding few microlitres of mustard oil (non toxic hydrophobic antibacterial) in biodegradable polymers such as PLGA (amorphous and relatively hydrophilic) and PLLA (semicrystalline and hydrophobic) compartments. Interestingly, minute quantity of mustard oil addition to either polymeric phase resulted in porosity in both phases, but predominantly in PLLA phase due to stronger affinity of mustard oil towards PLLA phase leading to hierarchically porous structure. Similar microstructures were also observed when the particles were loaded with dual actives such as antibacterial (benzoic acid (BA), hydrophilic) and antioxidant (tocopherol (TP), hydrophobic) in different polymeric phases. In addition to the synthesis, mechanism exploration, characterization, and the exploitation of these dual actives (antibacterial and antioxidant) loaded Janus as well as multi-layered particles as controlled release delivery vehicles for prolonging food shelf-life, are also demonstrated. This will open up a new strategy to build up particles with controlled architecture in a simplistic manner.

2. Experimental section

2.1. Materials

PLLA with intrinsic viscosity (I.V.) of 2.0 dL/g and PLGA (L:G = 50:50) with I.V. of 0.61 dL/g were bought from Sigma Aldrich, India. PLGA (L:G = 50:50) with I.V. of 1.1 dL/g was donated by Bezwada Biomedical Pvt. Ltd, USA. PLA with I.V. of 0.7 dL/g was bought from Natureworks, USA. Polyvinyl alcohol (PVA) (Mw: 125,000 g/mol, degree of hydrolysis: 89%) was procured from Chemical Drug House (CDH), India. Benzoic acid with purity: 99.6% and Tween20 were purchased from Merck, India whereas tocopherol was bought from TCI Chemicals, India. 2, 2-diphenyl picrylhydrazyl (DPPH) was purchased from Sigma Aldrich, India. Two polymeric dyes named as Poly(3-hexylthiophene-2,5-diyl) (Red) and Poly(9,9-di-*n*-octylfluorenyl-2,7-diyl)(Blue) were obtained from Sigma Aldrich, India. Dichloromethane (DCM) and methanol of HPLC grade were obtained from Fischer Chemicals, India. Antimicrobial activity of microparticles was studied against *Escherichia coli* (*E. coli*) *BL21 DE3 gold strain* which was bought from Agilent technologies, USA. For solid media preparation in petridish plates, nutrient agar and Luria broth (LB; liquid media for bacterial growth) was purchased from Hi-Media, India.

2.2. Fabrication of porous Janus/multilayered microparticles

Porous PLGA/PLLA Janus/multi-layered microparticles were synthesized using one-step emulsion solvent evaporation technique by varying the amount of mustard oil [43]. Before fabrication of particles, the respective cloud points for PLGA and PLLA phase were determined by following literature reported method [43] and given in Table 1 and Table ES1. PLGA and PLLA were individually dissolved in dichloromethane at a desired mass ratio of 2:1 or 1:2 and mustard oil was added into the PLGA solution. Both the polymer solutions were taken together and mixed for 5 min. To get a homogeneous polymer solution, solution was ultrasonicated for 1 min and poured into the previously stirring 0.5 wt% aqueous solution of PVA (maintaining O/W ratio of 0.02) using an overhead mechanical stirrer at 350 rpm. Then stirring was continued for 4 h to speed up the solvent evaporation. After 4 h of stirring, the particles were washed with distilled water and collected. Further, samples were dried using freeze drier and stored until further use. Similarly, the dual actives BA (antimicrobial) and tocopherol (antioxidant) encapsulated PLGA/PLLA microparticles with 50 μL mustard oil content were fabricated by incorporating appropriate quantity of actives in desired polymer solutions (Table 1 and Table ES1). Detailed description of sample characterizations and their applications as dual active delivery vehicles can be found in supporting information.

Table 1
Compositions, fabrication parameters, particle size and layer thickness for microparticles of various architecture.

Sample name	Type of polymers, viscosity (dL/g)	Amount of mustard oil (μL)	Particle size (μm)	Layer thickness (μm)		
				Shell/Smooth	Middle	Core/Rough
S1	PLGA: 0.61, PLLA: 2.0	0	415 ± 67	41 ± 10	85 ± 10	180 ± 13
S2	PLGA: 0.61, PLLA: 2.0	10	432 ± 34	40 ± 7	91 ± 6	115 ± 10
S3	PLGA: 0.61, PLLA: 2.0	50	448 ± 54	38 ± 3	92 ± 19	126 ± 17
S4	PLGA: 0.61, PLLA: 2.0	100	426 ± 40	31 ± 6	83 ± 10	203 ± 7
S5	PLGA: 0.61, PLLA: 2.0	125	421 ± 61	187 ± 50	–	201 ± 51
S6	PLGA: 0.61, PLLA: 2.0	150	414 ± 67	210 ± 48	–	217 ± 39
S7	PLGA: 0.61, PLLA: 2.0	50	526 ± 56	273 ± 68	–	259 ± 60
S8	PLGA: 1.10, PLA: 0.70	50	438 ± 72	42 ± 9	–	290 ± 27
S9	PLLA: 2.0, PLGA: 0.61	50	425 ± 55	99 ± 24	–	250 ± 14

Note: All systems were fabricated by taking 9 wt% polymer concentration (above cloud point of 8.5 wt%) except S8 which was fabricated at 8 wt% and cloud point was at 8 wt %. The mass ratio for shell to core polymer phases was kept at 2:1. In case of S7 and S8, 50 wt% BA in PLGA and 10 wt% TP in PLLA phase and in S9, 50 wt% BA in PLLA and 10 wt % TP in PLGA phase were added.

2.3. Characterizations of microparticles

2.3.1. Morphological analysis

Scanning electron microscope (SEM), ZEISS EVO50 was used to verify the surface as well as the bulk morphology of the particles. The cross-sectioning of all samples was done by using razor blade after dipping into the liquid nitrogen. Then, the sputter coater was used to coat the prepared microparticles before the SEM analysis. Image J software was used to measure particle size, layer thickness, pore size and particle/pore size distribution from SEM images by analyzing >100 particles. The morphologies of emulsion droplets during fabrication were observed by using optical fluorescence microscope (Leica DM2500).

2.3.2. Measurement of surface and interfacial tensions

Interfacial tensions between different polymer phases and aqueous solutions were determined using Tensiometer (K100, Krüss) following Du Noüy ring method. 4 wt% of each polymer (PLGA and PLLA) was dissolved in DCM and water phase was poured into the organic phase without disturbing the surface to make two separate layers. Then, the tensions at interface of both phases were measured using Tensiometer. All the experiments were performed in triplicates.

2.3.3. Determination of composition of layer and active distributions

Micro Raman spectrometer, GL127DW, UK was used to determine the layer or compartment compositions (type of polymer) as well as the distribution of actives in microparticles. All the particles were scanned under optical microscope using 20X lens and exposed to near infrared diode laser (785 nm) while keeping the scanning range of 2000–100 cm^{-1}. Different spots on the surface of microparticles were scanned through the point by point mapping. Further, layer configurations were determined using confocal laser scanning microscope (CLSM) (Leica TCS SP5 II) by incorporating poly(3-hexylthiophene-2,5-diyl) (Red dye) in PLGA phase and poly(9,9-di-*n*-octylfluorenyl-2,7-diyl)(Blue dye) in PLLA phase during fabrication. Polymeric dye loaded particles were scanned under CLSM to understand the layer disposition.

2.3.4. Thermal analysis

Thermal properties of microparticles were determined using differential scanning calorimetry, TA instrument, Q200. 5–7 mg of pre-dried samples were subjected to heating from 20 °C to 200 °C and cooled down to 20 °C at a heating/cooling rate of 10 °C/min respectively. Further, samples were heated up to 200 °C with a heating rate of 5 °C/min. Different thermal transitions like glass transition (T_g), cold crystallization (T_{cc}) and melting temperature (T_m) of microparticles in addition to percent crystallinity were recorded from the DSC plots.

2.3.5. In-vitro release study of dual actives

The diffusion of dual actives from multi-layered microparticles in PBS (pH 7) was studied at 37 °C and 200 rpm by following literature reported procedure [10]. 20 mg of each sample were taken into 5 mL of PBS solution and incubated using an incubator shaker. 2.5 mL of supernatant were extracted from the released medium after each time intervals and 2.5 mL of fresh PBS solution was replenished into the sample. The concentration of benzoic acid in extracted samples was measured using UV/Vis spectrophotometer (T90+, PG Instrument Ltd.) at λ_{max} of 226 nm. Similarly, the concentration of released tocopherol into the PBS buffer solution having 0.5%, w/v tween20, was determined using high performance liquid chromatography (HPLC, Shimadzu-SPD-20A, Japan) by maintaining methanol/water (98/2) mixture as mobile phase of and the samples were analyzed by UV/Vis detector at λ_{max} of 292 nm. Prior to the injection into HPLC column (C18 column), 2.5 mL of collected supernatant at each interval were extracted into DCM. After complete removal of DCM, 2 mL of methanol was added into the dried sample to dissolve the released tocopherol. Then the solution was filtered through 0.2 μm PTFE filter and injected into the HPLC column. The tocopherol content (retention time: 19 min) was determined by applying an appropriate calibration curve. The encapsulation efficiencies of benzoic acid and tocopherol for all the systems were calculated by following our previously published procedure [10]. All the experiments were executed in triplicates.

2.3.6. Hydrolytic degradation and water uptake study

To study the degradation of microparticles, 40 mg of each sample were suspended in 10 mL of PBS solution and kept at 37 °C and 200 rpm. After different time intervals, the degraded particles were filtered, collected and freeze dried. The morphology of dried samples was analysed using scanning electron microscope. Similarly, the % of water uptake study was carried out by taking 5 mg of microparticles in 2 mL of PBS solution [44]. All experiments were carried out in triplicates. After certain time interval of incubation, the samples were collected by filtration and weighed at wet conditions. Following that samples were dried in vacuum until it reached to a constant weight and then finally dry weight was noted. The water uptake % was determined for each time interval by following the equation given below: Water uptake (%) = 100% x $(W_{wet} - W_{dry})/W_{dry}$; W_{wet} = mass of wet particles and W_{dry} = mass of dried particles.

2.3.7. Evaluation of antimicrobial activity

The antibacterial activity of released active from the system S7, S8 and S9 were evaluated against *E. coli* in Luria broth (LB) media and bacterial cell growth was determined using plate spreading method [45]. Prior to that, the minimum inhibition concentration (MIC) for benzoic acid against *E. coli* was determined, which was found to be ~ 1750 μg/mL. Accordingly, the required amount of particles was calculated based on the released amount of benzoic acid in 24 h (following the data displayed in Fig. 5), which matches the MIC value and taken in 2 mL of LB solution. 1 mL of supernatant was extracted after predesigned time interval of incubation and fresh LB was replenished into the stock solution. From a freshly grown bacterial solution having cell concentration of 37×10^7 cells/mL, 10 μL were taken into the extracted samples and incubated at 37 °C and 200 rpm for 24 h. A control sample (LB solution without any particles) was also kept for incubation under similar conditions. The samples mixed with bacteria were diluted ranging from 10^1 to 10^{10} times in PBS. From each diluted samples, 50 μL were taken onto the solid nutrient agar petriplates and grown at 37 °C for 24 h. The number of surviving bacterial cells were counted and calculated as colony forming unit per mL (CFU/mL). Similar experiments were repeated for control sample also. All experiments were performed in triplicates. All the data were processed through one way ANOVA test and student *t*-test at different significant levels ($p < 0.05$, 0.01 and 0.001).

2.3.8. Estimation of antioxidant activity using DPPH radical scavenging assay

In order to study the antioxidant activity, the released tocopherol from microparticles S7, S8 and S9 were treated with DPPH solution and their radical scavenging efficiency was calculated by following Eq. (1) [46]. The desired amount of microparticles (same as taken for antibacterial study) was suspended in PBS solution having 0.5% (w/v) tween20 and incubated at 37 °C and 200 rpm. At different intervals of time, the released samples (0.5 mL) were extracted and fresh 0.5 mL of PBS solution was added into the sink. Further, the extracted sample was treated with freshly prepared 2.5 mL methanolic solution of DPPH (10^{-4} M) and kept in incubator shaker for 30 min at 37 °C. The absorbance of reduced DPPH solution due to the presence of released tocopherol was measured at 517 nm using UV/Vis spectrophotometer. At the same time, a blank experiment without any sample was also performed under similar conditions. The radical scavenging efficiency (expressed in %) of each sample was calculated using the following equation.

$$\text{Radical scavenging efficiency } (\%) = \frac{(A_{Control} - A_{Sample})}{A_{Control}} \times 100 \qquad (1)$$

where, $A_{control}$: absorbance of the control sample (without any microparticles), and A_{sample}: absorbance of reduced DPPH by released tocopherol from systems S7, S8 and S9. All experiments were performed in triplicates.

3. Results and discussions

3.1. Formation of multi-layered and Janus particles with varying porosity

Generally, it is difficult to control the phase separation of two immiscible components to generate particles with various architectures by adopting a simple oil-in-water (O/W) single emulsion system. It is even more challenging when the immiscible components are multiple (more than two). Interestingly, in this article, we have described a strategy by which microparticles with controlled morphology along with hierarchical porosity can be easily achieved by controlling the phase separation phenomena of three immiscible components (Scheme 1).

As illustrated in Fig. 1(a)–(d), Fig. 2(a)–(d) and ES1(a)–(d), a reference set of tri-layered particles composed of PLLA (I.V.: 2.0, middle layer) and PLGA (I.V.: 0.61, core and shell layer) (Table 1) were synthesized using one step emulsion solvent evaporation technique following our previously published article [10]. The influence of polymer viscosity to dictate the layer structure has been discussed in detail in another article to understand the formation of tri-layered structure out of two different polymers [47]. In order to make hierarchically porous multi-layered particles, mustard oil was incorporated only in the PLGA phase before being added into the emulsion. Because, we have demonstrated in our previous study that mustard oil can induce controlled porosity in PLGA based monophasic particles by influencing the interfacial tension and emulsion viscosity generated in W/O/W double emulsion [48,49]. So, it was thought to induce controlled porosity in PLGA layer of multilayered particles by incorporating mustard oil in PLGA phase only in an O/W based single emulsion. Unexpectedly, tri-layered structure with varying porosity in each layer was obtained till 100 μL of mustard oil addition (Table 2). Strikingly, porosity (porosity was calculated by following literature reported procedure [50]) was found to be higher at PLLA phase (e.g. S4, Fig. 2(d), middle layer's porosity-24.3 ± 2.6%, Table 2) as compared to PLGA phase (porosity ~2.8–4.0%) in which mustard oil was originally added. This indicates the significant migration of hydrophobic mustard oil towards PLLA phase (hydrophobic) due to stronger affinity between the two as compared to PLGA (relatively hydrophilic) phase. Interestingly, beyond 100 μL of mustard oil addition, Janus particles with hierarchical porosity were formed instead of multi-layered structure (Fig. 1(e), Fig. 2(e) and ES1(e–f)). The morphology of one half of Janus particles (S6) was observed to be rough and porous (pore size-9.9 ± 3.6 μm, Table 2), whereas other half was appeared to be smooth and porous but with reduced pore size (3.5 ± 1.8 μm, Table 2). Presumably, the rough and smooth compartments were made of semi-crystalline PLLA and amorphous PLGA phase respectively [51,52]. This was further confirmed from the solvent (THF) etching test (Figure ES2(b)). By dipping the particles in THF, selectively PLGA phase can be etched out keeping PLLA phase intact. The image displayed in Figure ES2(b) revealed the acorn type structure with a hollow core (inset of Figure ES2(b)) instead of completely phase separated bicompartments as shown in Figure ES2(c). The hollow core represents the trapped PLGA fraction inside the PLLA layer (discussed later). On the other hand, THF treated trilayered particles show hollow core with a shell (Figure ES2(a)) which actually the middle PLLA layer as observed in our previous publication [10]. Size of all sorts of particles (Janus and double-layered) and the porosity of each half were summarized in Tables 1 and 2 respectively. Particle sizes remain almost unchanged with the addition of mustard oil (S1-S6), though porosity varies (discussed below). This indicates the inclusion of tiny amounts of mustard oil did not significantly change the particle size.

3.2. Formation mechanism of porous multi-layered and Janus microparticles

The structural as well as morphological differences between multi-layered and Janus microparticles with hierarchical porosity induced by mustard oil can be explained with the help of classic spreading theory in combination with interfacial instability generated due to vanishing of interfacial tension at water/oil interface. Possibly, there are two distinct phenomena occurring simultaneously in the emulsion droplet: 1) spreading of one polymeric layer over another; and 2) pore formation onto the surface as well as inside the bulk of the layers. When the multiple polymer solutions,

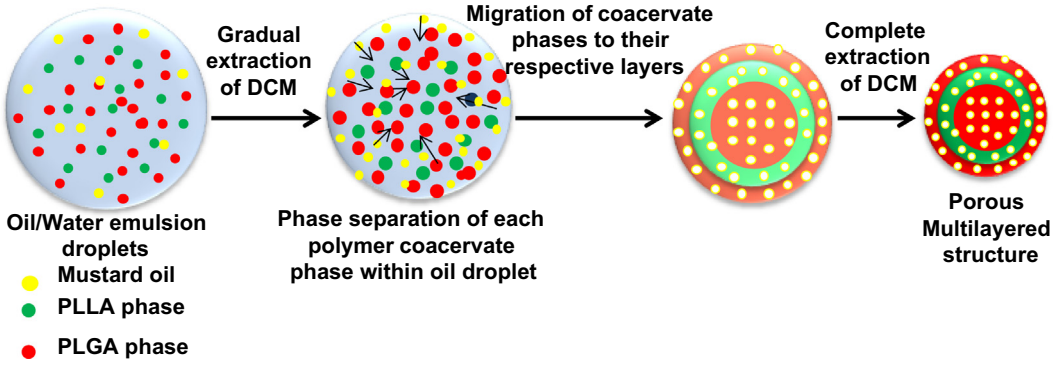

Scheme 1. Schematic representation for formation of porous multilayered microparticles using one-step solvent evaporation emulsion technique.

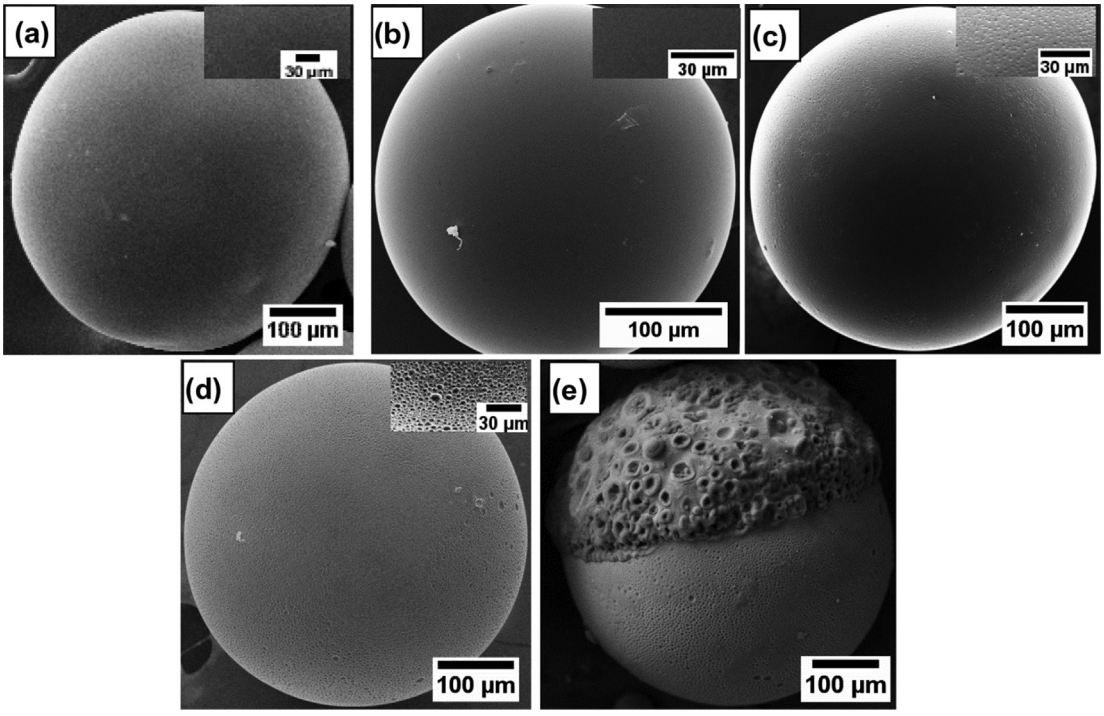

Fig. 1. Representative SEM images for the systems (a) S1, (b) S2, (c) S3, (d) S4, and (e) S6.

prepared above cloud point at which phase separation occurs, were added to PVA solution, the immiscible polymers were quickly phase separated and dispersed as discrete coacervate phases inside the primary emulsion droplets. These droplets also contain dissolved mustard oil in organic solvent (DCM). Due to rapid evaporation of solvent (DCM) that was diffused through the water phase, probability of solvent partitioning between each polymeric coacervate phase was low and hence, the interfacial tension between the individual polymer phases and also between the individual polymer phases with PVA solution may not vary significantly. This may result in a kinetically trapped tri-layered structure of non-equilibrium configuration dictated by their mass ratios (PLGA/PLLA = 2/1) [10] rather than following the spreading coefficient theory [53]. The shell and core of the tri-layers were made up of low viscous PLGA and middle layer was comprised of high viscous PLLA as confirmed from their corresponding Raman spectra (Figure ES3, discussed later). This has been observed for microparticles having no mustard oil [10] or very little amount of mustard oil (<20 µL). Under this condition, particles were produced with no or negligibly small porosity (Fig. 1(a,b), Fig. 2(a,b) and ES1(a-b)). However, pores were discernible at all the layers and inhomogeneously distributed all over the particles till the addition of 100 µL of mustard oil (Fig. 1(c,d), Fig. 2(c,d) and ES1(c,d), Table 2). Moreover, predominant accumulation of pores with bigger diameter (see the arrow in Fig. 2(d)) was evident in the middle layer presumably due to stronger affinity of mustard oil towards hydrophobic PLLA layer (cloud point for PLLA/mustard oil system (20 wt%), was significantly higher than that for PLGA/mustard oil (12.5 wt%)) [54].

Based on the combined information obtained from Figs. 1, 2 and Table 2, it can be inferred that porous tri-layered particles with non-uniform distribution of pores to all layers (including shell) were generated with progressively enhanced porosity till 100 µL of mustard oil addition (Fig. 2(c,d) and ES4 (Case-1), S3 and S4 in Table 2). Surprisingly, when concentration of mustard oil was reached to 125 µL or beyond, bicompartmental Janus particles were generated instead of multi-layered (Fig. 1(e), Fig. 2(e) and ES1(e-f)). Additionally, pore sizes were found to be much higher in one of the compartments (presumably PLLA, pore size: 9.9 ± 3.6 µm) as compared to the other (Table 2). This phenomenon can

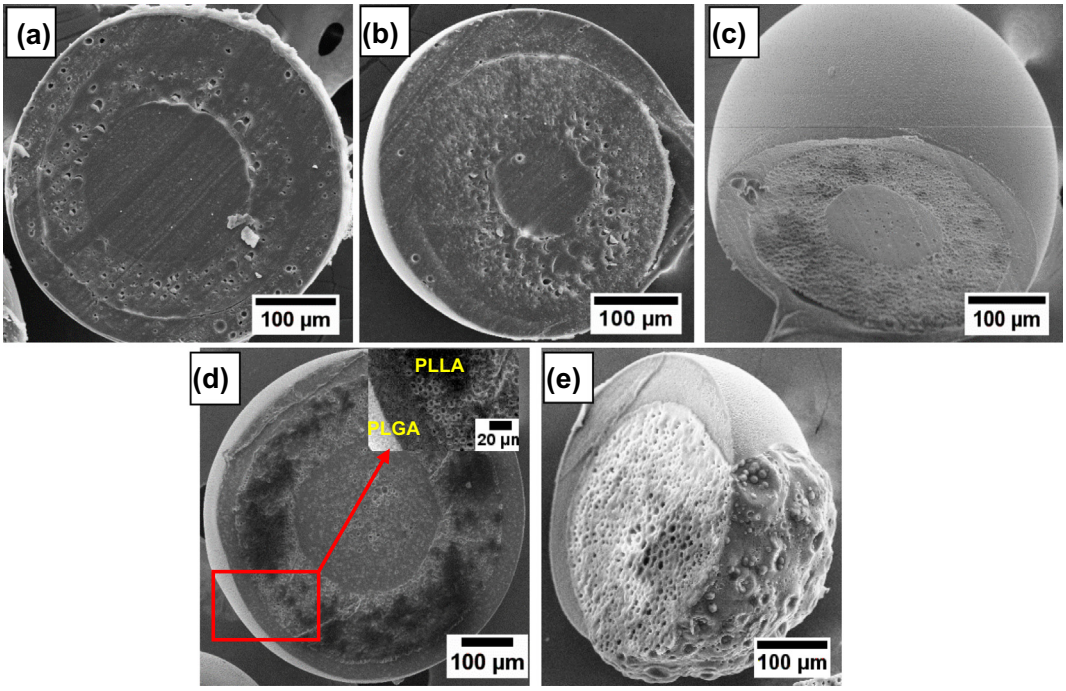

Fig. 2. Representative SEM images for cross-sectional view of samples (a) S1, (b) S2, (c) S3, (d) S4, and (e) S6.

Table 2
Particle size, layer thickness, pore characteristics, encapsulation efficiency (ee) for benzoic acid (BA) and tocopherol (TP) for microparticles.

Sample name	Internal pore size (μm)			Surface pore size (Smooth/Rough) (μm)	Porosity (%)*			ee	
	Shell/ Smooth	Middle	Core/ Rough		Shell/Smooth	Middle	Core/Rough	BA	TP
S3	–	3.1 ± 1.0	–	2.1 ± 0.9	–	19.3 ± 2.4	–	–	–
S4	2.1 ± 1.0	4.5 ± 1.3	2.1 ± 1.1	2.3 ± 1.1	4.0 ± 0.4	24.3 ± 2.6	2.8 ± 0.5	–	–
S6	2.6 ± 1.0	–	6.0 ± 2.5	3.5 ± 1.8/ 9.9 ± 3.6	8.9 ± 4.0	–	37.7 ± 3.8	–	–
S7	2.3 ± 1.2	–	5.2 ± 2.7	3.7 ± 1.3/ 7.2 ± 1.2	6.2 ± 1.24	–	30.3 ± 3.0	34.8 ± 0.3	84.7 ± 6.7
S8	1.2 ± 0.5	–	4.1 ± 1.5	1.7 ± 0.8	3.4 ± 0.3	–	17.0 ± 0.9	56.8 ± 2.6	69.1 ± 6.6
S9	4.7 ± 2.7	–	1.5 ± 0.8	6.5 ± 1.8	32.1 ± 2.9	–	5.3 ± 0.6	36.5 ± 2.4	78.7 ± 2.8

* Note: Porosity (%) was calculated using ImageJ software from 2D images as reported in literature [31].

partially be attributed to the dewetting transition coupled with interfacial instability originated due to the addition of mustard oil. In our previous study, we have demonstrated that addition of mustard oil into W/O/W double emulsion may substantially reduce interfacial tension between inner water and organic phase that may eventually generate porous particles [49]. In this case, when coacervate phases of individual polymers started coalescing to their respective phases to form tri-layered structure, the phase separated tiny mustard oil droplets may adsorb strongly at the PLLA/PLGA and outer PLGA/water interfaces in addition to distributing throughout the matrix. A similar phenomenon was also reported by Kim et al. [55]. In their work, they have shown how 2-methyl pentane can be adsorbed at water/oil interface similar to particle-stabilized emulsion (pickering emulsion) owing to fast extraction of DCM from the surface of emulsion droplets. However, in this study, the interface between middle layer (PLLA) and outer layer (PLGA) would also be crowded by mustard oil droplets owing to their stronger affinity towards PLLA layer as compared to PLGA layer. The PLLA layer would then undergo a transition from complete wetting by PLGA layer (due to high mass ratio of PLGA to PLLA) to partial wetting resulting in bicompartmental Janus particles. As per spreading coefficient theory, this occurs under a negative spreading coefficient of middle phase [41].

$$S_M = \gamma_{IO} - \gamma_{IM} - \gamma_{MO} < 0$$

where $\gamma_{IO}, \gamma_{IM}$and γ_{MO} represent interfacial tensions of the inner-outer, the inner-middle, and the middle-outer interfaces. S_M represents the spreading coefficient for the middle phase, a negative value of which implies that inner phase (middle layer) will eject out to come in contact with the outer phase due to reduced interfacial tension between inner (middle layer) and outer phase. In this case, PLLA (middle layer), PLGA (shell layer) and outer PVA solution were designated as inner, middle and outer phases (Figure ES4, Case-2). In order to find out the interfacial tension between each phases, a series of measurements were done and interfacial tension between PLLA layer and water solution in presence and absence of mustard oil were determined (Table ES2). Similar experiments were repeated for PLGA phase also (Tables ES3-ES4) and the results show that there is a significant reduction of interfacial tension between PLLA layer (and PLGA layer as well) and aqueous phase in presence of mustard oil (≥50 μL). Moreover, interfacial tension between PLLA layer and water phase was found to be comparatively lower in presence of mustard oil than that for PLGA layer (Tables ES2 and ES3-ES4). This clearly indicates that dewetting has been associated with the negative spreading coefficient generated by the mustard oil (Table 3(iii)). The calculated values of spreading coefficients based on the measured interfacial tension between each phase were tab-

Table 3
Interfacial tension measurements at different interfaces (PLGA(PG), PLLA(PL) 50 μL mustard oil (MO), 2% benzoic acid (BA), 10% tocopherol (TP) and PVA)and calculated spreading coefficient from equation.

SL No	Emulsion phase	γ_{IO}(mN/m)	γ_{IM} (mN/m)	γ_{MO} (mN/m)	S_I	S_M	S_O	Theoretical	Actual
i	PG0.6/MO/PVA	1.38	0.50	0.62	−1.26	+0.26	−1.50	CW	–
ii	PL2.0/MO/PVA	1.35	0.25	0.62	−0.98	+0.46	−1.71	CW	–
iii	PG0.6(MO)/PL2.0/PVA	1.56	0.63	1.35	−0.84	−0.42	−2.28	PW	CW[#]
iv	PG0.6(MO and BA)/PL2.0(TP)/PVA	1.47	0.63	1.10	−1.0	−0.26	−1.94	PW	PW
v	PG1.1(MO and BA)/PL0.7(TP)/PVA	1.36	0.69	0	−2.05	+0.67	−0.67	CW	CW
vi	PL2.0(MO and BA)/PG0.6(TP)/PVA	2.45	0.63	0	−3.08	+1.82	−1.82	CW	CW

[*]*Note:* Interfacial tensions were calculated by using following equation taking surface tensions of PLGA0.6, PLLA2.0 with 26.63 and 24.57mN/m and for high viscous PLGA 1.1 dL/g and PLA 0.7 dL/g were measured values 23.4 and 27.2 mN/m respectively and 19.81 mN/m for mustard oil.
$\gamma_{12} = \gamma_1 + \gamma_2 - 2\Phi\sqrt{\gamma_1\gamma_2}$
$\gamma_{12} = \left(\sqrt{\gamma_1} - \sqrt{\gamma_2}\right)^2$
Where,γ_1, γ_2 and Φ are the surface tensions for different phases and volume fraction respectively.

ulated in Table 3 and S_M was found to be negative (Table 3(iii)). This essentially shows the protrusions of inner phase (PLLA layer) on surface of the particle were thermodynamically favorable. Probably, the mustard oil droplets worked as 'particle-stabilized emulsion' stabilizer (akin to pickering emulsion) (Figure ES4, Case-2). In another possibility, after fast evaporation of low boiling DCM, the emulsion droplets became increasingly mustard oil (boiling point-170 °C, solubility in water <1%) rich reducing the solvent quality for the coacervate polymer phases which started to precipitate and coalesced with their respective phases. When the two proximal interfaces of individual layers (PLLA and PLGA) were populated with mustard oil droplets, attractive adhesion energy (F) between the PLLA-PLGA interface and PLGA-outer interfaces was generated. This adhesion energy may also induce a dewetting transition to make Janus particles (Figure ES4, Case-2) [41]. Mustard oil droplet induced reduction of interfacial tension between PLLA layer and aqueous phase may actually reinforce the adhesion energy and favor the dewetting. Apart from interfacial tension, viscosity of droplets may also play a role in favoring dewetting transition. Because the miscibility of mustard oil in PLLA was significantly higher than that in PLGA layer as judged from cloud point experiments [54], the PLLA interface should be enriched with mustard oil droplets after rapid evaporation of DCM. This may further enhance the viscosity [49] of already viscous (high molecular weight, IV: 2.0) PLLA layer leading to the migration of PLLA layer towards water layer triggering a dewetting transition as illustrated schematically in Case-2 of Figure ES4. Similar attraction induced dewetting transition was observed for emulsion droplets stabilized by amphiphillic diblock copolymer, which underwent dewetting due to the addition of less volatile poor solvent [56]. In order to further elucidate formation of the Janus particles, structural evolution of the primary emulsion droplets with progressive solvent evaporation was periodically monitored under optical microscope (Fig. 3). As shown in Fig. 3(i-v), in presence of minute quantity of mustard oil (~50 μL), the initially formed core-shell structure of multi-layered particles remained unchanged over time. However, after addition of >125 μL of mustard oil, dewetting transition of initially formed core-shell structure of multilayered particles was clearly evident in Fig. 3(vi-x). At low or zero concentration of mustard oil, the initially generated polymeric coacervate phases meet the criteria of complete wetting (Figure ES4 (Case-1)) [47] and hence, core-shell structure with PLGA as shell and PLLA as inside layer was produced (Figs. 1 and 2(a–d). It is worth mentioning here that a fraction of PLGA was trapped as inner core inside PLLA layer of these tri-layered particles (see the arrows in Fig. 3(i-v)) as evidenced by the formation of hollow core after selective dissolution of PLGA layer with THF (Figure ES2(a)) [57]. However, for the samples with 150 μL mustard oil content (S6), with the progressive evaporation of DCM, the concentrations of PLGA, PLLA and mustard oil increase accompanying with the decrease of γ_{IO}(Table ES3-ES4). This triggers the inversion of S_M from positive to negative leading to dewetting transition (Fig. 3(vi-x), and ES4 (Case-2) Table 3(iii)). It is noteworthy that the movement of trapped PLGA fractions inside the viscous PLLA layer would be highly slowed down, which can be distinctly visible under optical microscope as shown by the arrows in Fig. 3(-vii-viii) and hence, coalescence of it with outside PLGA fractions would be prohibited. This would lead to an acorn structure where outside PLGA would partially engulf PLLA layer inside of which PLGA core would be trapped (Fig. 1(e) and 2(e)).

At high concentration of mustard oil (150 μL), the PLLA (middle layer) and PLGA (shell layer) layers would migrate towards the opposite directions and a clear interface slowly builds up at the centre leading to the formation of Janus structure (S6, Fig. 3(vi-x)), though core PLGA fraction may still be entrapped inside PLLA layer. This phenomenon was also clearly evident at low concentration of mustard oil with the addition of BA (see the arrows in Fig. 3(xi-xv), discussed later). Apart from this, the Janus particles with completely phase separated PLGA and PLLA domain without entrapment of a fraction of PLGA core inside PLLA layer were also produced (Figures ES1(n-o) and ES5(a-d)). This was observed either with the combination of high viscous PLGA (I.V.: 1.1) and high viscous PLLA (I.V.: 2.0) (SB-6, Figures ES5(c-d)) or with a pair of low viscous PLGA (I.V.: 0.61) and low viscous PLA (I.V.: 0.7) (SB-5, Figures ES5(a-b)). The key to achieve perfect Janus particles would be to add mustard oil into a perfect double layered structure instead of tri-layered structure.

In addition to additives (mustard oil, BA (discussed later)) which alter interfacial tension, physical characteristics of polymers such as hydrophobicity, molecular weight/viscosity of polymer, percent crystallinity, T_g etc. also play a pivotal role in the interfacial behavior and the final microstructure of the particle. For example, anisotropic roughness (and porosity as well) on the surface of semi-crystalline PLLA based Janus particles was clearly evident from SEM images (Fig. 4(a) and (d)). Moreover, double-layered particles (obtained by tweaking viscosity and mass ratio of PLGA and PLLA phases [47]) containing PLLA as shell layer (S9) also display uneven rough surface (Fig. 4(c)) as compared to particles (systems S1-S4) comprised of amorphous PLGA as shell layer (Fig. 1(a–d)). The formation of rough surface for S9 particles was also observed by optical microscope (Fig. 3(xxi-xxv)). Apparently, this could be attributed to the interfacial instability which usually generates wrinkled surface caused by vanishing of interfacial tension at oil/water interface [58]. In this study, phase separated mustard oil droplet would probably distribute both on the shell (PLLA and/or PLGA) and interior of the particles as well. In case of Janus particles, these droplets would also crowd at the interface of migrated PLLA layer and PVA solution due to extremely low interfacial tension generated between the two, much akin to particles stabilized emulsion (Tables 3, ES2 and ES3). This may trigger interfacial instability that may lead to interfacial roughening [41]. But, interfacial

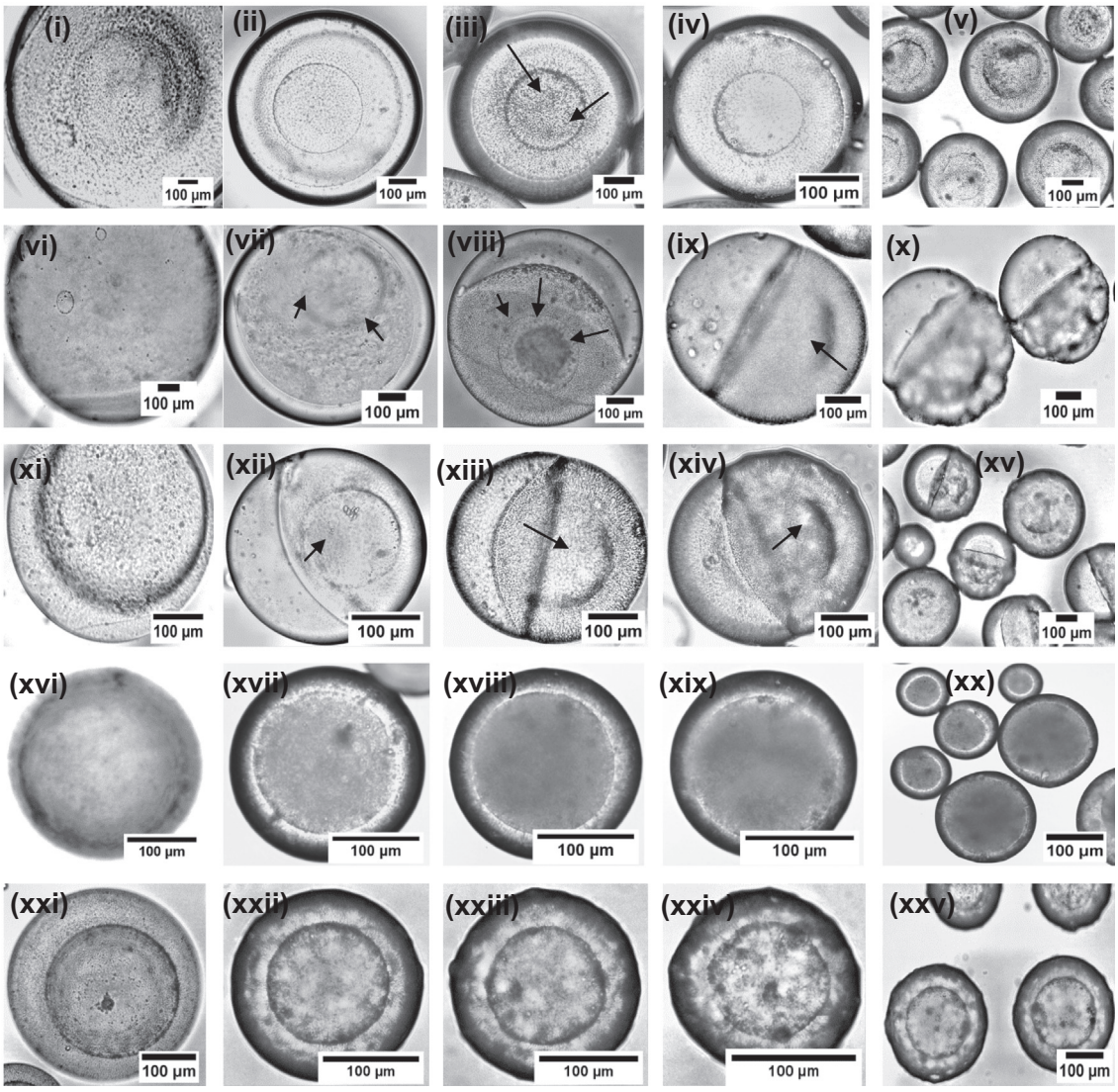

Fig. 3. Optical images of microparticles during fabrication of S3 (i), (ii), (iii), (iv) and (v), S6 (vi), (vii), (viii), (ix) and (x), S7 (xi), (xii), (xiii), (xiv) and (xv), S8 (xvi), (xvii), (xviii), (xix) and (xx) and S9 (xxi), (xxii), (xxiii), (xxiv) and (xv) taken after 0, 5, 10, 15 and 40 min of stirring, respectively.

roughening should be highly suppressed for the chosen polymers because of their high intrinsic viscosity and enhanced entanglement originated from high molecular weight chain [58]. Thus, ideally, wrinkles on the surface due to interfacial roughening should not arise for PLGA (molecular weight >50 K for both grades of PLGA) and PLLA layers (molecular weight >200 K) as well with the addition of mustard oil. Therefore, both PLGA and PLLA layers would produce smooth surfaces even in presence of mustard oil droplet. Moreover, double layered particles with zero mustard oil content were also observed to produce rough surface when PLLA remained as shell layer [59]. In summary, particles (in Janus/acorn/multi-layer) in which PLLA layer directly interacts with aqueous phase, would give rise to rough surfaces irrespective of the mustard oil content whereas PLGA layers under the similar circumstances resulted in smooth surface. Hence, interfacial roughening may not be the reason of producing this anisotropic roughness in Janus and/or layered particles. This roughening phenomenon could then be attributed to the crystallinity of PLLA phase (~40% crystallinity, Table ES5) which underwent shrinkage at a faster rate during solvent evaporation compared to the amorphous PLGA phase. Similar phenomena have been reported by us in our previous study [10,52] and others as well [59].

Interfacial instability may not lead to interfacial roughening as explained above, but it might be partially responsible for generation of porous structure on the surface of the particles as explained below. With the rapid evaporation of DCM, the concentration of polymers as well as mustard oil droplet increases and phase separated tiny mustard oil droplet may adsorb at the primary emulsion droplet/water interface in addition to PVA (stabilizer) [55]. This may lead to a dramatic reduction of interfacial tension between water and emulsion droplets (Table ES2-ES4). The progressive decrease of interfacial tension between water and organic phase (comprised of PLLA or PLGA in DCM) with the addition of mustard oil clearly supports the hypothesis (Table ES(3–4)). Extremely low or zero interfacial tension between the two phases may trigger an increase in surface area of the emulsion droplet to adopt a microemulsion structure at the expense of negligible free energy penalty [60,61]. This may lead to infiltration of few small water droplets from outer water phase into the PLLA/PLGA containing organic phase droplet to form W/O/W double emulsion stabilized by both mustard oil and PVA. This phenomenon is clearly evident from fluorescence optical microscopic images of the emulsion droplets (Figure ES6). To understand the water droplet insertion into DCM phase, green colored fluorescein dye was incorporated in

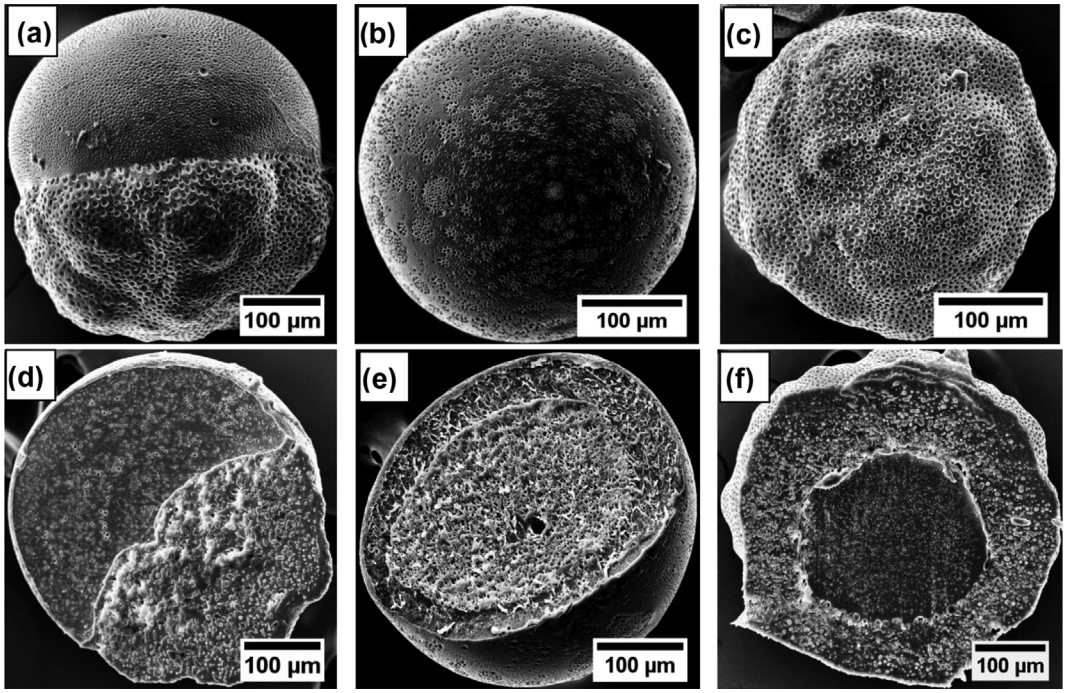

Fig. 4. SEM images for the loaded particles (a) S7, (b) S8, (c) S9, and cross-sectional images of (d) S7, (e) S8 and (f) S9.

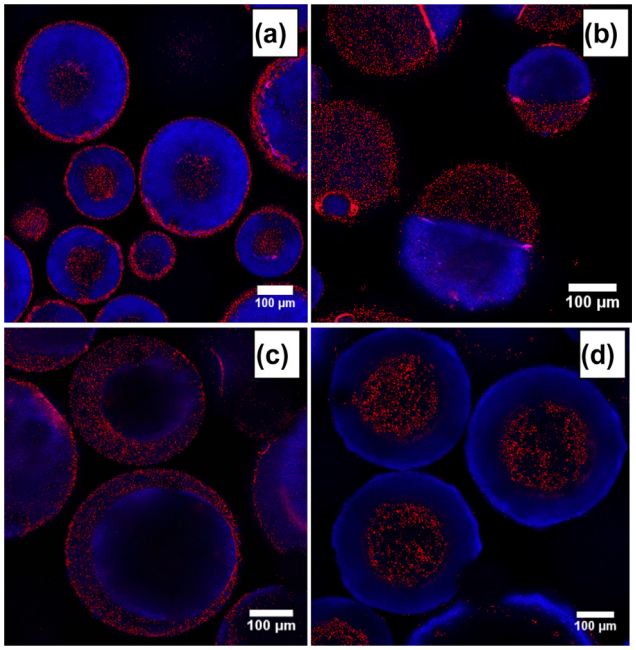

Fig. 5. Confocal laser scanning microscopic images for (a) S3, (b) S7, (c) S8 and (d) S9 containing red dye (Poly(3-hexylthiophene-2,5-diyl)) in PLGA and blue dye (Poly (9,9-di-*n*-octylfluorenyl-2,7-diyl) in PLLA phase.

the water phase. Figure ES6(b) shows few small green colored water droplets (see arrows) inside the emulsion droplet indicating the formation of W/O/W double emulsion that resulted in the porous structure after complete evaporation of DCM as well as water. These green colored water droplets were not observed inside the emulsion droplet with zero mustard oil content (Figure ES6(a)). This reveals the role of mustard oil as porogen which primarily induced interfacial instability between water and organic phase leading to the formation of microemulsion structure that eventually formed pores. Similar observation related to pore formation caused by interfacial instability owing to synergistic adsorption of surfactant and block copolymer at water/oil interface was also reported by Ku et al. [62].

In addition to interfacial instability, pore formation mechanism can partly be ascribed to the phase separation of mustard oil from the polymeric matrix followed by volume contraction after solidification. Initially, mustard oils along with the polymers were soluble in DCM. With the progressive evaporation of solvent, quality of solvent will decrease. Thus, the concentration of polymers as well as mustard oil will increase. This may lead to the formation of tiny droplet of mustard oil due to reduction of solubility of mustard oil in DCM in addition to incompatibility of mustard oil with the polymers. These phase separated mustard oil droplets were uniformly distributed inside the emulsion droplet. Upon further removal of solvent, mustard oil droplets may coalesce to make pores that could be trapped inside the viscous polymer matrix irrespective of shell or core (Fig. 2). These pores were not observed for particles having zero mustard oil content (Figs. 1 and 2(a)). Apart from this, concentration of mustard oil played a pivotal role to tune the pore size and pore density in addition to pore distribution. Due to low concentration of mustard oil, the time for phase separation to form tiny mustard oil droplets would be increased without affecting much of polymer precipitation rate. Instead of coalescence, this may cause trapping of these tiny mustard oil droplets inside the viscous polymer matrix after solidification. Therefore, porosity and pore sizes were found to be progressively lower for particles with less content of mustard oil (Table 2). Moreover, due to high boiling point, mustard oil droplets may not leave the surface rather it may get entrapped into the polymer matrix. NMR study revealed the presence of mustard oil residue in the freeze-dried particles (data not shown) [49]. Emulsion droplets containing low T_g (Table ES5), amorphous PLGA ($T_g \sim 50$ °C, which will be even lower after solvation [63,64]) would remain soft so that phase separated mustard oil droplets gathered at shell may form pores after volume contraction upon solvent evaporation, but would give rise to smooth surface. On the other hand, high

T_g (Table ES5), semicrystalline PLLA (63 °C) would rather produce rough surface with bigger pores (Fig. 1 and Table 2). Presumably, roughness on PLLA surface may primarily arise due to self-organization of crystalline chains during solvent evaporation [51]. In addition to the trapping of mustard oil droplets, the porosity in PLLA layer can further be caused by the space between layers of the crystalline lamella that may lead to enhanced pore size on PLLA surface (porosity ~20–32%) as compared to PLGA surface (porosity ~3–8%, Table 2) [65].

In our previous work, we have demonstrated the simultaneous release of two actives (hydrophilic antibacterial and hydrophobic antioxidant) from multilayered particles which were proved to be a potential solution for prolonging shelf-life of food [10]. In this article, we were interested to see how the release profiles of these actives would be influenced when they were encapsulated in these types of porous Janus or porous multilayered particles. In order to make dual actives loaded multi-layered porous particles (under similar condition as used for the preparation of S3), initially BA (hydrophilic antibacterial) and tocopherol (hydrophobic antioxidant) were incorporated in PLGA and PLLA phases respectively along with the addition of 50 μL mustard oil in PLGA phase. Surprisingly, instead of multi-layered porous particles, Janus porous particles were generated (S7, Fig. 4(a) and (d)). Unlike sample S6, completely phase separated compartment of the Janus particles were comprised of PLLA and PLGA respectively as confirmed from Raman spectra (Figure ES3(b)) and THF etching (Figure ES2(c)) test which shows complete removal of one half of the spheres. This indicates the abrupt change of interfacial tension between PLLA and PLGA phases in presence of tocopherol and BA, which may probably facilitate the dewetting even in presence of minute quantity of mustard oil. The reduction of interfacial tension between PLGA or PLLA and water phases were clearly evident in presence of BA [66] (Table ES2-ES4). Moreover, porosity and pore sizes of each compartment were also changed significantly (Table 2) as compared to unloaded particles (S3). Presumably, accumulation of BA along with mustard oil at water/organic interface reduces the interfacial tension which may lead to enhanced porosity as shown in Table 2. In addition, enhancement of crystallinity in PLLA phase after addition of BA (as observed from DSC data, Figure ES7 and Table ES5) may further facilitate the pore formation with bigger size due to increased space between crystalline lamella and shrinkage after solidification. Upon further addition of mustard oil keeping BA and tocopherol constant (SB1-SB4, Table ES1), only Janus porous particles were resulted in with increasingly bigger pore size (from ~ 2–4 μm in PLGA and ~ 6–8 μm in PLLA phase, Figure ES1(j-m), Table ES1). This shows how Janus particles with tunable porosity can be easily achieved by varying mustard oil content. In order to make porous bilayered/core–shell particles, instead of PLGA, PLLA phase was taken in higher amount (mass ratio of PLLA/PLGA = 2/1) keeping all other parameters constant and porous particles with bi-layered morphology (S9) were created (Fig. 4(c) and (f)) as confirmed from THF etching and Raman spectra (Figure ES2(e) and ES3(d)). This clearly indicates that in addition to interfacial tension, emulsion viscosity also played a crucial role to dictate the final morphology [47]. As viscosity of PLLA (I.V.: 2.0) was much higher than that of PLGA (I.V.: 0.61), the dewetting and migration of inside layer (PLGA) towards aqueous phase were prohibited (Fig. 3(xvi-xx)). To confirm this hypothesis, in the next experiment, high viscous PLGA (IV: 1.1 dL/g) and same PLLA (I.V.: 2.0) in 2:1 mass ratio (PLGA/PLLA = 2/1) were used keeping all other parameters constant and as expected, Janus porous particles (SB5, Table ES1, Figure ES1(n)) were only generated. Similarly, Janus particles were also resulted in under the same conditions, when the viscosity of PLGA (I.V.: 0.61) and PLA phase (I.V.: 0.7) were close (SB6, Table ES1, Figure ES1(o)). In order to achieve core–shell particles with PLGA as shell layer, low viscous PLA (I.V.: 0.7) was chosen in combination with high viscous PLGA (I.V.: 1.1) keeping all the other parameters constant including PLGA/PLA mass ratio (2/1) and finally, porous double layered particles were yielded with PLGA being in the shell and PLA in the core as confirmed by Raman spectroscopy (discussed later) and solvent (THF) etching (Figure ES2(d)) experiment which shows loss of shell instead of core. The formation of S8 particles can be seen in the optical microscopic images (Fig. 3(xvi-xx)). It is worth mentioning here that the surfaces of these double layered particles (S8, Fig. 4(b)) appeared patchy probably due to the slight migration of PLA phase towards outside aqueous phase [41]. Irrespective of the compositions and architecture, all types of particles display varying porosity in each layer (Table 2).

The configuration of each layer/compartment was further confirmed using confocal Raman microspectroscopy (Figure ES3) and it was clear from the spectra that the shell and core were PLGA (characteristic broad band at 873 cm^{-1} and a doublet at 1425 cm^{-1} and 1454 cm^{-1} for —CH_2 stretching from the lactide and glycolide segments [67] respectively) and PLLA (characteristic sharp band at 873 cm^{-1} and a singlet at 1425 cm^{-1}) abundant regions respectively for S8 (Figure ES3(c)) and vice-versa for S9 (Figure ES3(d)). Similar spectral differences were found from bicompartmental particles (S7, Figure ES3(b)) in which smooth and rough compartments corresponded to PLGA and PLLA dominant phases, respectively. In the spectra obtained from sample S7, appearance of a sharp peak at 1003 cm^{-1} corresponding to BA in PLGA phase and two characteristic peaks at 480 cm^{-1} and 587 cm^{-1} corresponding to tocopherol in PLLA phase verified the predominant distribution of BA and tocopherol in their respective phases only. Similarly, in case of S8 and S9, the characteristic peaks for additives (BA and tocopherol) were found in desired locations (Figure ES3(c,d)). Apart from these, layer segregation in appropriate manner was further confirmed by capturing CLSM images of the selected particles with various architectures. Prior to that, blue and red polymeric dyes (Figure ES8) were incorporated in PLLA and PLGA phases respectively during fabrication and the images were captured and displayed in Fig. 5. The CLSM images from tri-layered (S3), Janus/bi-compartmental (S7), bi-layered (S8) and inverse-bi-layered (S9) samples revealed the layer configurations which match well with the results obtained from SEM and Raman study. Interestingly, blue and red dyes did not mix with each other in any of the samples indicating the coexistence of well-separated phases in desired fashion. To further investigate the phase separation and influence of entrapped actives (in addition to layer formation) on the T_g and crystallinity of the polymers, thermal characterizations using differential scanning calorimetry (DSC) were conducted for selective particles. The DSC plots for all the samples (S3, S7, S8 and S9) were compared (Figure ES7) and summarized in Table ES5. In all cases, two endothermic transitions were appeared at ~50 °C and ~60 °C, attributed to the T_g of PLGA and PLLA or PLA, respectively revealing their biphasic behavior, though the combination of these polymers usually form miscible blend with a single T_g [51]. Also, T_gs (T_{cc} and T_m as well) obtained from the particles remained almost unchanged as compared to the corresponding pure polymers (Table ES5). However, a significant increase in % crystallinity of PLLA phase was observed especially in active loaded particles (S7-55% and S9-57%) irrespective of the positioning of PLLA layer (side compartment or shell). This might happen due to heterogeneous nucleation of PLLA chain on the surface of BA (probably migrated from PLGA phase for sample S7) implying a strong interaction (via H—bonding) between the two [45,52]. On the contrary, disappearance of T_{cc} and depreciation of % crystallinity of PLA in sample S8 (Figure ES7) as compared to its native state reveal the difficulty in aligning of PLA chains because of its positioning as core.

3.3. In vitro release study

In order to compare the effect of layer configuration on the release behaviors, release behaviors of BA (antibacterial) and tocopherol (antioxidant) from samples S7-S9 were studied in PBS buffer solution (pH 7) at 37 °C [68,69] and the release profiles were plotted in Fig. 6. The encapsulation efficiency of both actives were determined and tabulated in Table 2 for all the samples. Being a hydrophilic active, encapsulation efficiency of BA was comparatively lower compared to hydrophobic tocopherol irrespective of the samples. Being in the shell (for layered particles) or side compartment (for Janus particles), the release of hydrophilic BA was significantly faster compared to hydrophobic tocopherol (remain in core or in side compartment) regardless of the nature of particles. However, the releases of both actives were observed to be sustained and controlled with a highly suppressed initial burst. Compared to the samples S7 and S8, rate of BA release from sample S9 was appreciably higher during initial period (first 10 days) of release study. The differences in release behaviours can be explained with the help of surface porosity (Fig. 4, ES1(g-i) and Table 2) and water uptake data as well (Figure ES9). As seen from Fig. 4(c) and (f), S9 comprised of highly porous but highly viscous PLLA (I.V. 2.0 dL/g) shell with large pore size (Table 2) due to migration of hydrophobic mustard oil into PLLA phase due to stronger affinity of former to the later. A porous layer would always have a tendency to facilitate water ingression that would rapidly dissolute entrapped BA and release them [70,71]. However, after releasing 35–40% of BA in 10 days, the release rate became sluggish and continued till 60 days in controlled manner. This implies the initial release of actives were from the surface of the particles. And in later days, actives were released from the bulk which comprised of highly viscous, semi-crystalline and slow degrading PLLA layer that may eventually decelerate the active release. Water uptake data for S9 displayed in Figure ES9 followed the similar trend (discussed later). Strikingly, the faster and continuous release of BA was achieved from Janus particles (S7) owing to its predominant confinement in less viscous, amorphous and easily degradable porous PLGA (IV: 0.61) compartment. However, for the double-layered S8 particles, the high viscous (IV: 1.1) and less porous PLGA shell (pore size-1.7 ± 0.8 μm) provided a relatively strong barrier to the diffusion of BA entrapped predominantly in the shell, thus retarding the active release. Further, to investigate about the active-release mechanism from S7-S9 microparticles, the famous Ritger-Peppas model [72,73] was used (Figure ES10) and the calculated kinetic parameters were tabulated in Table ES6. Based on the outcome of the model (see supporting information for the detailed discussion), dual active release from S7 was found to follow diffusion controlled mechanism after initial burst, whereas S8 and S9 predominantly follow diffusion in combination with erosion controlled pathway.

The release profiles of the microparticles of various architectures can also be explained with the help of water uptake data (Figure ES9) and the hydrolytic degradation study of the particles shown in Fig. 7. High initial water influx was observed in double layered S9 particles owing to the existence of highly porous (large pore size- 6.5 ± 1.8 μm and porosity 32.1 ± 2.9%, Table 2) PLLA shell. The higher water ingression probably accelerated the release of surface entrapped BA leading to rapid release of BA during initial period (Fig. 6). Moreover, enhanced water uptake through porous PLLA shell sped up the degradation of low viscous, amorphous (easy to degrade) PLGA core (Fig. 7(k–o)), disappearance of which was evident after 20 days in Fig. 7(l). Disappearance of characteristic peaks related to PLGA and existence of only peaks relevant to PLLA layer were evident in Raman spectra of degraded particles (Figures ES11(e,f)). Presumably, aqueous soluble oligomers produced from degraded PLGA core may diffuse towards the outer water phase and leach out through the porous PLLA shell resulting in rapid release of BA (hydrophilic). However, the retard release of tocopherol (present in the core) from sample S9 indicates the strong Van der Waals interaction between the tocopherol [10]

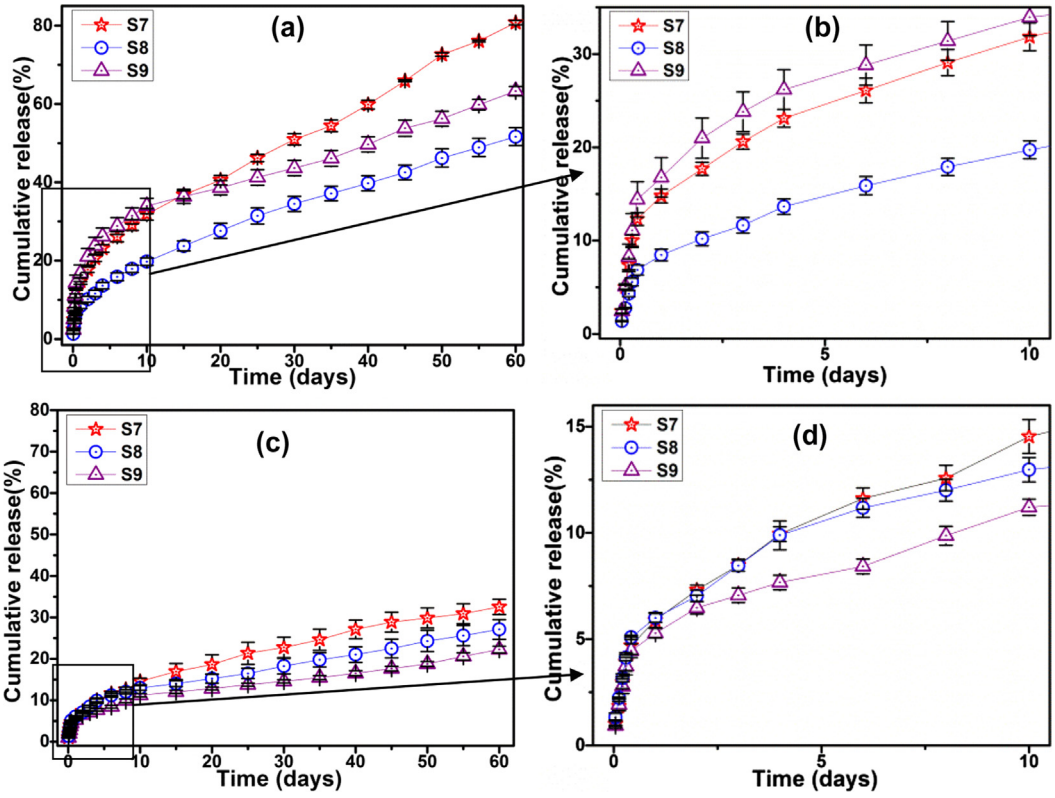

Fig. 6. In vitro release profiles for (a) benzoic acid ((b) zoom in for 10 days) and (c) tocopherol ((d) zoom in for 10 days) from systems S7, S8 and S9.

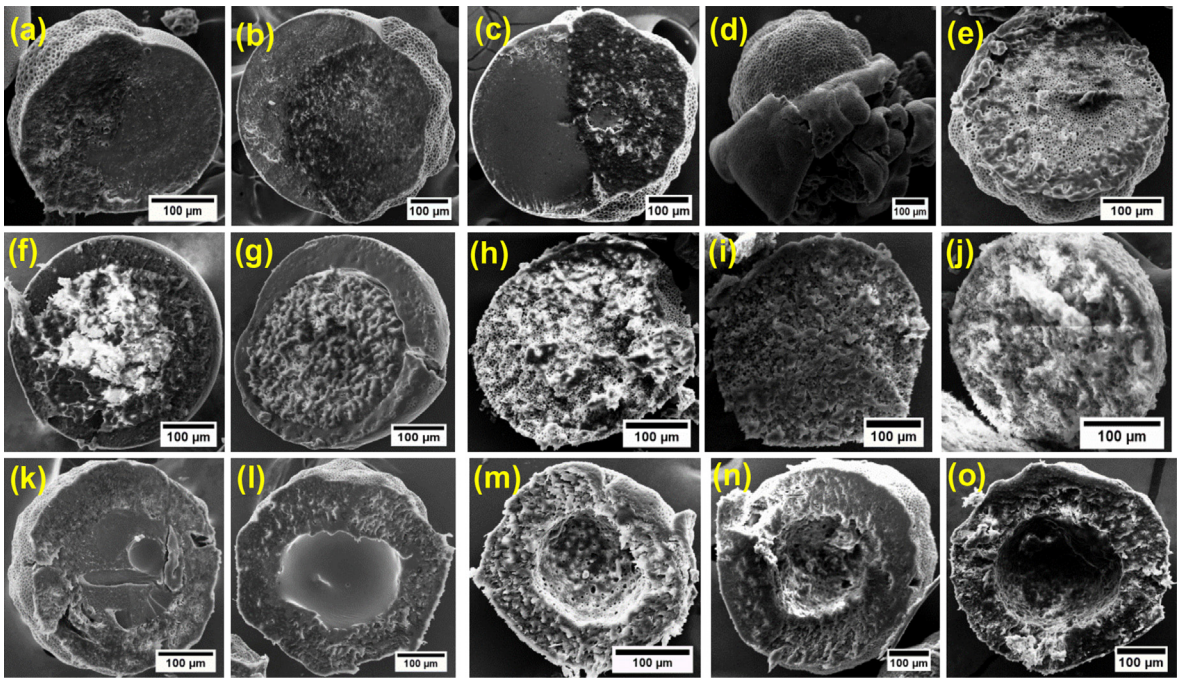

Fig. 7. Representative SEM images of degraded microparticles from systems S7, S8 and S9 after (a), (f), (k) 10 days, (b), (g), (l) 20 days, (c), (h), (m) 30 days, (d), (i), (n) 40 days and (e), (j), (o) 60 days of incubation, respectively.

and hydrophobic PLLA shell. Moreover, the pores of PLLA were probably surrounded by a tiny layer of hydrophobic mustard oil that may additionally hinder the release of hydrophobic tocopherol. Low water uptake in late stage (Figure ES9) and non-degraded layer of PLLA shell even after 60 days explain the sluggish release of both actives from these bi-layered particles (especially after removal of PLGA core within 20 days). Interestingly, Janus particles provided fastest, but controlled and sustained release of both actives owing to their high water uptake (Figure ES9). High water influx through the pores of both compartments (PLGA and PLLA) resulted in an increased water uptake which accelerated the diffusion of active towards water phase. In Janus particles, BA was predominantly present in low viscous, amorphous and porous PLGA compartment, the degradation of which should be accelerated by rapid water ingression. On the contrary, high water uptake did not enhance the degradation of either phase (not even PLGA phase) till 30 days (Fig. 7(c)) as shown in Fig. 7(a–e). Presumably, the bulk degradation of easily degradable PLGA compartment was also slow due to its high thickness (layer thickness of PLGA compartment: 273 ± 68 µm) as compared to other particles (layer thickness of PLGA ~ 40 µm, Table 1) in which surface erosion would be predominant over bulk degradation [74], thus achieving faster mass loss of PLGA in bi-layered (Fig. 7(f–o)) and tri-layered particles (shown in our previous study) [10]. This indicates the rapid release of dual actives from Janus particles was predominantly diffusion controlled instead of degradation controlled as predicted from Power law model (Figure ES10). Partial degradation of PLGA layer was evident only after 40 days of incubation resulting in mushroom type particles as shown in Fig. 7(d) while PLLA layer remained intact till 60 days (Fig. 7(e)). The preferential removal of PLGA compartment shows the anisotropic degradation of one compartment over other. This can easily be achieved by selecting right combination of polymer pair as shown in this study. Finally, the morphology of the particles resembles pure PLLA after 60 days of incubation indicative of the complete degradation of PLGA compartment as evidenced from Raman spectra as well (Figures ES11 (a,b)). On the other hand, double-layered S8 particles containing high viscous PLGA as shell, exhibited slowest release of both actives as compared to other particles. The slow release of both actives correlates well with its lowest water uptake data (Figure ES9). With the introduction of high viscous PLGA (I.V.: 1.1 dL/g) shell of lower porosity (Table 2) to the bi-layered PLGA/PLLA particles, the degradation of PLGA shell was sluggish and the shell remained intact even after 20 days of incubation arising from low water influx (Fig. 7(f–j)). Moreover, after partial removal of PLGA shell within 30 days, the relatively hydrophobic and semi-crystalline PLLA core remained almost unaffected even after 60 days (Fig. 7(j)), though with enhanced pores (~75% increase of pore size (~7.2 ± 1.05 µm)). The disappearance of PLGA shell keeping PLLA core intact was also confirmed from their corresponding Raman spectra taken after 10 and 60 days (Figures ES11(c-d)). It is worth noting here that for sample S8, trapped PLLA patches in the PLGA shell may further retard water influx that would not only reduce shell degradation rate, but also decrease the active diffusion towards the release medium. Therefore, the slower degradation of shell as well as core in combination with low water uptake gave rise to sluggish release of both actives as compared to other particles. In summary, among all the samples, the high water ingression caused the faster but controlled release of dual actives from Janus particles via diffusion controlled mechanism.

3.4. Antimicrobial activity

The prolonged antibacterial activity of dual active loaded systems S7, S8 and S9 were evaluated against *E. coli* using plate spreading method [45] by following our previously published protocol. Prior to the experiment, the MIC (minimum inhibitory concentration) value at which the complete inhibition of bacterial growth occurs for the free BA were determined against *E. coli* and it was found to be around 1750 µg/mL [10]. The particle concentrations used for the antibacterial activity study were calculated from their release kinetics on the basis of released amount of BA (equivalent to MIC) in 24 h (Fig. 6(a)). As displayed in Fig. 8, the sustained antibacterial activity was achieved for all the systems over a period of 2 months due to controlled and continuous release of BA. Initially, the bacterial growth inhibition

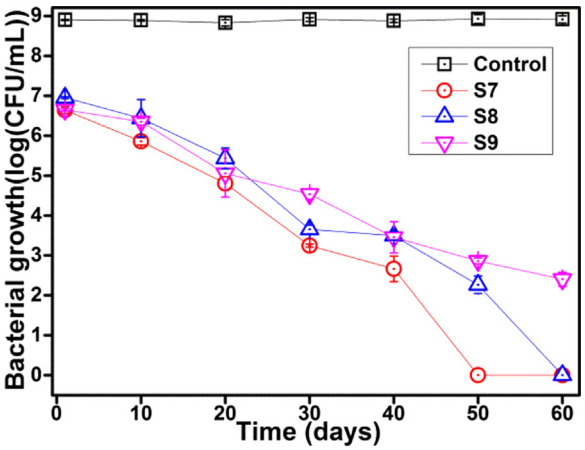

Fig. 8. Evaluation of antibacterial activity of systems S7, S8 and S9 against *E. coli*.

remained almost same (~2 log(CFU/mL)) irrespective of the sample compositions due to the similar amount of BA release during initial 24 h. However, in late stage, Janus particles (S7) showed the best antibacterial activity (~5 log(CFU/mL) after 30 days) among all the samples presumably due to faster release of BA from the porous Janus particles as shown in Fig. 6. It is worth mentioning that the similar antibacterial activity was achieved in our previous study from tri-layered particles (S1 with zero mustard oil content) at a double particle concentrations compared to these mustard oil loaded systems (S7-S9) [10]. However, mustard oil may not have directly contributed towards the antibacterial property of the particles as shown in our previous study [48,49]. The superior antibacterial property demonstrated by Janus particles was probably due to the consequences of faster and sustained release of BA in combination with degraded residues (oligomers) of PLGA/PLLA, which are known to be antibacterial in nature, as discussed in our previous study [48,49]. It is important to note that all the antibacterial activity data were processed through the one way ANOVA analysis and *t*-test keeping the significant level P value <0.05, 0.01 and 0.001.

3.5. Antioxidant activity

In order to investigate antioxidant activity of the dual active loaded particles, radical scavenging assay using diphenylpicrylhydrazyl (DPPH) was carried out by following literature reported method [75]. Good antioxidant activity (~70–90%) for prolonged period of time (60 days) was demonstrated by all the samples irrespective of their compositions (Fig. 9). This could be attributed to

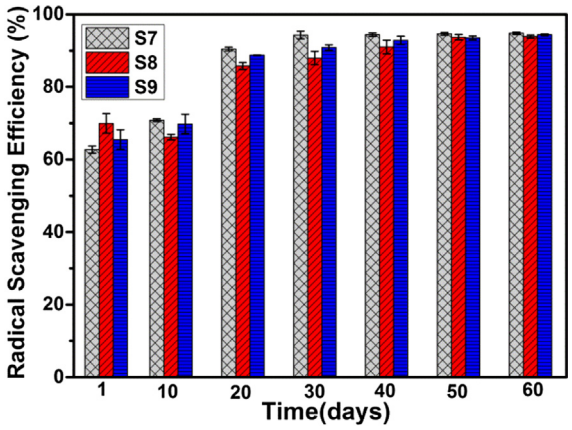

Fig. 9. Antioxidant activities of S7, S8 and S9 systems.

the slow and controlled release of tocopherol from core of the particles. Among the all systems, being in the side compartment, Janus particles provided relatively faster release of tocopherol, thus achieving slightly better radical scavenging efficiency compared to others especially at late stages. Similar trend was also observed in the case of antibacterial property. In summary, it can be stated that the dual active loaded microparticles of various architectures with desirable antimicrobial and antioxidant property for prolonged period of time have been achieved by simple oil in water emulsion technique by incorporating few microlitres of mustard oil. These particles will have immense potential to act not only as controlled release packaging materials but also as drug delivery vehicles.

4. Conclusions

Based on the knowledge gained from previously reported articles published by us and others [10,38,47,49], we have developed a novel and facile strategy to fabricate PLGA/PLLA based multilayer and Janus microparticles with hierarchically porous structure simply by the addition of non toxic mustard oil into oil-in-water based single emulsion. The formation mechanism of the particles with various configurations and varying porosity were thought to be primarily originated from the change of interfacial tension between different polymeric phases induced by mustard oil. The particle formation mechanism has been established with the help of in situ optical microscopic study and interfacial tension measurements. It was revealed that the emulsion viscosity and change of interfacial tensions primarily induced by additives such as mustard oil and benzoic acid as well, are the main causes for the particles to adopt various configurations such as Janus to multilayer. Moreover, the porosity of the particles was found to be varied with the mustard oil content and significantly higher in semi-crystalline, hydrophobic PLLA phase as compared to PLGA phase. This could be attributed to predominant localization of hydrophobic mustard oil in the PLLA phase that may undergo crystallinity induced shrinkage resulting in pore formation. In addition, interfacial instability and mustard oil induced phase separations were also considered to be responsible factors for pore formation. Further, we have demonstrated the potential application of these particles by entrapping multiple food packaging actives (benzoic acid as antibacterial and tocopherol as antioxidant) in different phases and releasing them in controlled and sustainable fashion aiming for long shelf life of food. Janus particles with hierarchical porosity were found to provide most desirable release kinetics as compared to multilayered particles for prolonged period of time (60 days). The various configurations adopted by the biodegradable particles may find their applications in several areas ranging from drug delivery, catalysis, sensor to food packaging. Currently, an effort is underway in our lab to produce nanoparticles with similar architectures by optimizing the emulsion parameters so as to exploit them as drug delivery vehicles too.

CRediT authorship contribution statement

Agni Kumar Biswal: Methodology, Data curation, Formal analysis, Investigation, Writing - original draft. **Sampa Saha:** Conceptualization, Writing - review & editing, Supervision.

Declaration of Competing Interest

The authors declare that they have no known competing financial interests or personal relationships that could have appeared to influence the work reported in this paper.

Acknowledgement

The research has been supported by 'SERB' with a grant id of EEQ/2016/000455.

Appendix A. Supplementary material

Supplementary data to this article can be found online at https://doi.org/10.1016/j.jcis.2020.01.071.

References

[1] A. Walther, A.H.E. Müller, Janus particles: synthesis, self-assembly, physical properties, and applications, Chem. Rev. 113 (7) (2013) 5194–5261.
[2] S. Jiang, Q. Chen, M. Tripathy, E. Luijten, K.S. Schweizer, S. Granick, Janus particle synthesis and assembly, Adv. Mater. 22 (10) (2010) 1060–1071.
[3] J. Shi, Y. Jiang, X. Wang, H. Wu, D. Yang, F. Pan, Y. Su, Z. Jiang, Design and synthesis of organic–inorganic hybrid capsules for biotechnological applications, Chem. Soc. Rev. 43 (15) (2014) 5192–5210.
[4] J. Cui, M.P. van Koeverden, M. Müllner, K. Kempe, F. Caruso, Emerging methods for the fabrication of polymer capsules, Adv. Coll. Interf. Sci. 207 (2014) 14–31.
[5] D. Velasco, E. Tumarkin, E. Kumacheva, Microfluidic encapsulation of cells in polymer microgels, Small 8 (11) (2012) 1633–1642.
[6] S. De Koker, L.J. De Cock, P. Rivera-Gil, W.J. Parak, R. Auzély Velty, C. Vervaet, J. P. Remon, J. Grooten, B.G. De, Geest, Polymeric multilayer capsules delivering biotherapeutics, Adv. Drug Del. Rev. 63 (9) (2011) 748–761.
[7] G.B. Sukhorukov, A. Fery, M. Brumen, H. Möhwald, Physical chemistry of encapsulation and release, Phys. Chem. Chem. Phys. 6 (16) (2004) 4078–4089.
[8] S. Saha, S.C.J. Loo, Recent developments in multilayered polymeric particles - from fabrication techniques to therapeutic formulations, J. Mater. Chem. B 3 (17) (2015) 3406–3419.
[9] S. Saha, S.C.J. Loo, Application-driven multi-layered particles – The role of polymers in the architectural design of particles, Polymer 71 (2015) A1–A11.
[10] A.K. Biswal, S. Saha, Prolonging food shelf-life by dual actives release from multi-layered polymer particles, Coll. Surf. B Biointer. 175 (2019) 281–290.
[11] S. Saha, D. Copic, S. Bhaskar, N. Clay, A. Donini, A.J. Hart, J. Lahann, Chemically controlled bending of compositionally anisotropic microcylinders, Angew. Chem. Int. Edit. 51 (3) (2012) 660–665.
[12] S. Rahmani, S. Saha, H. Durmaz, A. Donini, A.C. Misra, J. Yoon, J. Lahann, Chemically orthogonal three-patch microparticles, Angew. Chem. 126 (9) (2014) 2364–2370.
[13] S. Ifra, Saha, Fabrication of topologically anisotropic microparticles and their surface modification with pH responsive polymer brush, Mater. Sci. Eng. C 104 (2019) 109894.
[14] A. Walther, A.H.E. Müller, Janus particles, Soft Matter 4 (4) (2008) 663–668.
[15] J. Hu, S. Zhou, Y. Sun, X. Fang, L. Wu, Fabrication, properties and applications of Janus particles, Chem. Soc. Rev. 41 (11) (2012) 4356–4378.
[16] F. Liang, C. Zhang, Z. Yang, Rational design and synthesis of Janus composites, Adv. Mater. 26 (40) (2014) 6944–6949.
[17] S. Rahmani, J. Lahann, Recent progress with multicompartmental nanoparticles, MRS Bulletin 39 (3) (2014) 251–257.
[18] T. Nisisako, T. Torii, Formation of biphasic Janus droplets in a microfabricated channel for the synthesis of shape-controlled polymer microparticles, Adv. Mater. 19 (11) (2007) 1489–1493.
[19] D. Dendukuri, S.S. Gu, D.C. Pregibon, T.A. Hatton, P.S. Doyle, Stop-flow lithography in a microfluidic device, Lab on a Chip 7 (7) (2007) 818–828.
[20] C. Kaewsaneha, P. Tangboriboonrat, D. Polpanich, M. Eissa, A. Elaissari, Preparation of Janus colloidal particles via Pickering emulsion: An overview, Coll. Surf. A Physicochem. Eng. Asp. 439 (2013) 35–42.
[21] J.P. Rolland, B.W. Maynor, L.E. Euliss, A.E. Exner, G.M. Denison, J.M. DeSimone, Direct fabrication and harvesting of monodisperse, shape-specific nanobiomaterials, J. Am. Chem. Soc. 127 (28) (2005) 10096–10100.
[22] A. Walther, X. André, M. Drechsler, V. Abetz, A.H.E. Müller, Janus discs, J. Am. Chem. Soc. 129 (19) (2007) 6187–6198.
[23] H.Y. Chen, J.M. Rouillard, E. Gulari, J. Lahann, Colloids with high-definition surface structures, Proc. Natl. Acad. Sci. 104 (27) (2007) 11173–11178.
[24] S.S. Yu, C.L. Chang, C.R.C Wang Lee, Gold nanorods: Electrochemical synthesis and optical properties, J. Phys. Chem. B 101 (34) (1997) 6661–6664.
[25] K. Esumi, K. Matsuhisa, K. Torigoe, Preparation of rodlike gold particles by UV irradiation using cationic micelles as a template, Langmuir 11 (9) (1995) 3285–3287.
[26] V.M. Cepak, C.R. Martin, Preparation and stability of template-synthesized metal nanorod sols in organic solvents, J. Phys. Chem. B 102 (49) (1998) 9985–9990.
[27] B.R. Martin, D.J. Dermody, B.D. Reiss, M. Fang, L.A. Lyon, M.J. Natan, T.E. Mallouk, Orthogonal self-assembly on colloidal Gold-Platinum nanorods, Adv. Mater. 11 (12) (1999) 1021–1025.
[28] S. Fullam, D. Cottell, H. Rensmo, D. Fitzmaurice, Carbon nanotube templated self-assembly and thermal processing of Gold nanowires, Adv. Mater. 12 (19) (2000) 1430–1432.
[29] N.R. Jana, L. Gearheart, C.J. Murphy, Seed-mediated growth approach for shape-controlled synthesis of spheroidal and rod-like gold nanoparticles using a surfactant template, Adv. Mater. 13 (18) (2001) 1389–1393.
[30] J.W. Kim, R.J. Larsen, D.A. Weitz, Synthesis of nonspherical colloidal particles with anisotropic properties, J. Am. Chem. Soc. 128 (44) (2006) 14374–14377.
[31] J.W. Kim, R.J. Larsen, D.A. Weitz, Uniform nonspherical colloidal particles with tunable shapes, Adv. Mater. 19 (15) (2007) 2005–2009.
[32] T. Tanaka, M. Okayama, Y. Kitayama, Y. Kagawa, M. Okubo, Preparation of "Mushroom-like" Janus particles by site-selective surface-initiated atom transfer radical polymerization in aqueous dispersed systems, Langmuir 26 (11) (2010) 7843–7847.
[33] H. Yu, M. Chen, P.M. Rice, S.X. Wang, R.L. White, S. Sun, Dumbbell-like bifunctional Au−Fe3O4 nanoparticles, Nano Letters 5 (2) (2005) 379–382.
[34] W.L. Lee, S.C.J. Loo, Revolutionizing drug delivery through biodegradable multilayered particles, J. Drug Target. 20 (8) (2012) 633–647.
[35] W. Tong, X. Song, C. Gao, Layer-by-layer assembly of microcapsules and their biomedical applications, Chem. Soc. Rev. 41 (18) (2012) 6103–6124.
[36] B.G. Mathapa, V.N. Paunov, Fabrication of novel cyclodextrin-polyallylamine hydrochloride co-polymeric microcapsules by templating oil-in-water emulsions, Soft Matter 9 (19) (2013) 4780–4788.
[37] A.R. Abate, M. Kutsovsky, S. Seiffert, M. Windbergs, L.F.V. Pinto, A. Rotem, A.S. Utada, D.A. Weitz, Synthesis of monodisperse microparticles from non-Newtonian polymer solutions with microfluidic devices, Adv. Mater. 23 (15) (2011) 1757–1760.
[38] W. Li, H. Dong, G. Tang, T. Ma, X. Cao, Controllable microfluidic fabrication of Janus and microcapsule particles for drug delivery applications, RSC Adv. 5 (30) (2015) 23181–23188.
[39] M.T. Gokmen, F.E. Du Prez, Porous polymer particles-A comprehensive guide to synthesis, characterization, functionalization and applications, Prog. Polym. Sci. 37 (3) (2012) 365–405.
[40] Q. Peng, H. Cong, B. Yu, L. Wei, K. Mahmood, H. Yuan, R. Yang, X. Zhang, Y. Wu, Preparation of polymeric Janus microparticles with hierarchically porous structure and enhanced anisotropy, J. Colloid Interf. Sci. 522 (2018) 144–150.
[41] X. Huang, Q. Qian, Y. Wang, Anisotropic particles from a one-pot double emulsion induced by partial wetting and their triggered release, Small 10 (7) (2014) 1412–1420.
[42] H.C. Shum, J.W. Kim, D.A. Weitz, Microfluidic fabrication of monodisperse biocompatible and biodegradable polymersomes with controlled permeability, J. Am. Chem. Soc. 130 (29) (2008) 9543–9549.
[43] W.L. Lee, Y.C. Seh, E. Widjaja, H.C. Chong, N.S. Tan, S.C. Joachim Loo, Fabrication and drug release study of double-layered microparticles of various sizes, J. Pharm. Sci. 101 (8) (2012) 2787–2797.
[44] W.L. Lee, M. Hong, E. Widjaja, S.C.J. Loo, Formation and degradation of biodegradable triple-layered microparticles, Macromol. Rap. Comm. 31 (13) (2010) 1193–1200.
[45] A.K. Biswal, M. Usmani, S.Z. Ahammad, S. Saha, Unveiling the slow release behavior of hollow particles with prolonged antibacterial activity, J. Mater. Sci. 53 (8) (2018) 5942–5957.
[46] Z. Aytac, T. Uyar, Antioxidant activity and photostability of α-tocopherol/β-cyclodextrin inclusion complex encapsulated electrospun polycaprolactone nanofibers, Eur. Polym. J. 79 (2016) 140–149.
[47] A.K. Biswal, S. Saha, New insight into the mechanism of formation of dual actives loaded multilayered polymeric particles and their application in food preservation, J. Appl. Polym. Sci. 136 (40) (2019) 48009.
[48] A.K. Biswal, M. Usmani, S.Z. Ahammad, S. Saha, Synergistic combinations of natural antimicrobials encapsulated in the porous PLGA particles and their application in food preservation, Indian Patent (201711035034) (201711035034).
[49] A.K. Biswal, P. Hariprasad, S. Saha, Efficient and prolonged antibacterial activity from porous PLGA microparticles and their application in food preservation, Mater. Sci. Eng. C 108 (2020) 110496.
[50] C. Grove, D.A. Jerram, jPOR: An ImageJ macro to quantify total optical porosity from blue-stained thin sections, Comp. Geosci. 37 (11) (2011) 1850–1859.
[51] A.K. Parthipan, N. Gupta, K. Pandey, B. Sharma, J. Jacob, S. Saha, One-step fabrication of bicompartmental microparticles as a dual drug delivery system for Parkinson's disease management, J. Mater. Sci. 54 (1) (2019) 730–744.
[52] N. Gupta, A.K. Biswal, A.K. Parthipan, B. Kaur, B. Sharma, J. Jacob, S. Saha, Bicompartmental microparticles loaded with antibacterial agents for prolonging food shelf life, J. Mater. Sci. 54 (13) (2019) 9729–9744.
[53] K.J. Pekarek, J.S. Jacob, E. Mathiowitz, One-step preparation of double-walled microspheres, Adv. Mater. 6 (9) (1994) 684–687.
[54] Determination of cloud point-200 mg of polymer (4 wt%) and 150 μL of mustard oil dissolved in 5 mL of DCM in 10mL measuring cylinder and kept for solvent evaporation. Cloud point was calculated in weight% from the remaining volume of polymer solution where the phase separation occured.
[55] M.R. Kim, S. Lee, J.K. Park, K.Y. Cho, Golf ball-shaped PLGA microparticles with internal pores fabricated by simple O/W emulsion, Chem. Comm. 46 (39) (2010) 7433–7435.
[56] H.C. Shum, E. Santanach-Carreras, J.W. Kim, A. Ehrlicher, J. Bibette, D.A. Weitz, Dewetting-induced membrane formation by adhesion of amphiphile-laden interfaces, J. Am. Chem. Soc. 133 (12) (2011) 4420–4426.
[57] W.L. Lee, W.L. Foo, E. Widjaja, S.C.J. Loo, Manipulation of process parameters to achieve different ternary phase microparticle configurations, Acta Biomater. 6 (4) (2010) 1342–1352.

[58] S. Liu, R. Deng, W. Li, J. Zhu, Polymer microparticles with controllable surface textures generated through interfacial instabilities of emulsion droplets, Adv. Funct. Mater. 22 (8) (2012) 1692–1697.
[59] W.L. Lee, C. Loei, E. Widjaja, S.C.J. Loo, Altering the drug release profiles of double-layered ternary-phase microparticles, J. Controlled Release 151 (3) (2011) 229–238.
[60] R. Granek, R.C. Ball, M.E. Cates, Dynamics of spontaneous emulsification, J. de Phys. II. 3 (6) (1993) 829–849.
[61] R. Granek, Spontaneous curvature-induced rayleigh-like instability in swollen cylindrical micelles, Langmuir 12 (21) (1996) 5022–5027.
[62] K.H. Ku, J.M. Shin, D. Klinger, S.G. Jang, R.C. Hayward, C.J. Hawker, B.J. Kim, Particles with tunable porosity and morphology by controlling interfacial instability in block copolymer emulsions, ACS Nano 10 (5) (2016) 5243–5251.
[63] A. Yoshioka, K. Tashiro, Solvent effect on the glass transition temperature of syndiotactic polystyrene viewed from time-resolved measurements of infrared spectra at the various temperatures and its simulation by molecular dynamics calculation, Macromolecules 37 (2) (2004) 467–472.
[64] F. Mohamed, C.F. van der Walle, PLGA microcapsules with novel dimpled surfaces for pulmonary delivery of DNA, Int. J. Pharm. 311 (1) (2006) 97–107.
[65] Y. Asano, K. Nakayama, S. Yao, Creation of functional materials by use of a slow crystallization process in the nonequilibrium state. I. porous polyamide microparticles, J. Appl. Polym. Sci. 90 (9) (2003) 2428–2432.
[66] J.J. Jasper, T.D. Wood, The surface pressure of soluble benzoic acid films at water-halobenzene interfaces, J. Phys. Chem. 60 (12) (1956) 1625–1627.
[67] H. Yan, Y.F. Hou, P.F. Niu, K. Zhang, T. Shoji, Y. Tsuboi, F.Y. Yao, L.M. Zhao, J.B. Chang, Biodegradable PLGA nanoparticles loaded with hydrophobic drugs: confocal Raman microspectroscopic characterization, J. Mater. Chem. B 3 (18) (2015) 3677–3680.
[68] C. Fuciños, P. Fuciños, L.M. Pastrana, M. Rúa, Functional characterization of poly(N-isopropylacrylamide) nanohydrogels for the controlled release of food preservatives, Food Bioproc. Technol. 7 (12) (2014) 3429–3441.
[69] A.S. Glaive, T. Modjinou, D.L. Versace, S. Abbad-Andaloussi, P. Dubot, V. Langlois, E. Renard, Design of antibacterial and sustainable antioxidant networks based on plant phenolic derivatives used as delivery system of carvacrol or tannic acid, ACS Sustain. Chem. Eng. 5 (3) (2017) 2320–2329.
[70] X. Huang, C.S. Brazel, On the importance and mechanisms of burst release in matrix-controlled drug delivery systems, J. Control. Release 73 (2) (2001) 121–136.
[71] W.L. Lee, E. Widjaja, S.C.J. Loo, One-step fabrication of triple-layered polymeric microparticles with layer localization of drugs as a novel drug-delivery system, Small 6 (9) (2010) 1003–1011.
[72] P.L. Ritger, N.A. Peppas, A simple equation for description of solute release I. Fickian and non-fickian release from non-swellable devices in the form of slabs, spheres, cylinders or discs, J. Control. Release 5 (1) (1987) 23–36.
[73] B. Surnar, M. Jayakannan, Stimuli-responsive poly(caprolactone) vesicles for dual drug delivery under the gastrointestinal tract, Biomacromol. 14 (12) (2013) 4377–4387.
[74] H.K. Makadia, S.J. Siegel, Poly lactic-co-glycolic acid (PLGA) as biodegradable controlled drug delivery carrier, Polymers 3 (3) (2011) 1377–1397.
[75] V.M.D. Mambro, A.E.C.S. Azzolini, Y.M.L. Valim, M.J.V. Fonseca, Comparison of antioxidant activities of tocopherols alone and in pharmaceutical formulations, Int. J. Pharm. 262 (1) (2003) 93–99.